International Journal of Computational Intelligence Systems
Vol. **14(1)**, 2021, *pp.* 1714–1727
DOI: https://doi.org/10.2991/ijcis.d.210608.001; ISSN: 1875-6891; eISSN: 1875-6883
https://www.atlantis-press.com/journals/ijcis/

Research Article

A Distributed Urban Traffic Congestion Prevention Mechanism for Mixed Flow of Human-Driven and Autonomous Electric Vehicles

Chenn-Jung Huang[1,2,*], Kai-Wen Hu[2], Hsing Yi Ho[1], Bing Zhen Xie[1], Chien-Chih Feng[1], Hung-Wen Chuang[1]

[1]*Department of Computer Science and Information Engineering, National Dong Hwa University, Hualien, 974301, Taiwan*
[2]*Department of Electrical Engineering, National Dong Hwa University, Hualien, 974301, Taiwan*

ARTICLE INFO

Article History
Received 14 Jan 2021
Accepted 31 May 2021

Keywords
Support vector regressions
Optimization
Intelligent transportation systems
Autonomous mobility-on-demand
Congestion control
Machine learning

ABSTRACT

Traffic congestion in urban areas has become a critical problem that municipal governments cannot overlook. Meanwhile, mixed traffic systems containing both autonomous and human-driven electric vehicles ramp up the challenge for traffic management in urban areas. Although numerous researchers have proposed traffic control heuristics to alleviate traffic congestion problems in the recent literature, scant research has addressed the joint problems of route and charging strategies for electric vehicles along with urban traffic congestion prevention. Accordingly, this work tackles the complex task of traffic management in urban areas during peak periods by using practical congestion prevention strategies that consider the characteristics of mixed traffic flows and the charging demands of electric vehicle users. Notably, we apply support vector regressions to compute the charging time at each charging point and the traverse time of an electric vehicle at each road segment/intersection, based on historical traffic data. The simulation results reveal that the proposed algorithms are feasible because they can avoid possible occurrences of traffic congestion during rush hours and provide the routes and charging options that are chosen by electric vehicle users.

1. INTRODUCTION

The world has experienced dramatic urbanization in recent decades. In 1950, only 30% of the world's total population lived in cities. However, following the baby boom after the Second World War, dramatic global population expansion has been accompanied by concentration of populations in cities. The latest United Nations statistical report [1] estimates that by 2050, the global population will surge to 9.7 billion, with 68% of the population living in urban areas. This means the problems of traffic congestion, traffic accidents, and air pollution caused by rapidly increasing numbers of vehicles and population growth in urban areas cannot be ignored. Although the central and local governments of many countries have proposed various traffic management plans to alleviate traffic congestion in urban areas, huge volumes of privately owned vehicles simultaneously traversing specific popular road segments during commute times still causes inconvenience and serious economic losses for most societies.

In recent years, many vehicle users have come to rely on vehicle navigation systems installed in their automobiles to recommend less-congested routes they can follow instead of taking the shortest paths. However, as illustrated in [2], widespread usage of vehicle navigation systems often leads to network state oscillations and makes traffic congestion worse. Meanwhile, the congestion problem is exacerbated further by the unpredictability of driving behavior and fluctuating traffic conditions during commute times. In the recent literature, although researchers have presented route reservation mechanisms to prevent road traffic congestion in urban areas [3], vehicle reservation cancellations were not considered in those studies. In addition, early and late vehicle arrivals at the road segments caused by prediction errors also tended to weaken the congestion control effect.

Besides the traffic congestion problem, owing to concern over greenhouse gas emissions, many countries have announced and promoted policies to ban the sale of fossil fuel-powered vehicles, and plan to prohibit the sale of some or all such vehicles in the next few decades. Electric vehicles (EVs) that use green energy to reduce carbon emissions are currently recognized as the best alternative to traditional automobiles in the future. However, an important issue to be solved in the future development of EVs is the convenience of EV charging. Most EVs are currently charged at charging stations, homes or workplaces. Due to the limited capacity of EV batteries, if their storage capacity is insufficient, EVs need to find a charging station on the route for replenishment.

Driven by the upsurge in the popularity of EVs, self-driving technology has received more attention than ever. Although the two are completely different technologies that do not need to be combined, and both can operate independently, the major reason

*Corresponding author. Email: cjhuang@gms.ndhu.edu.tw

why automakers have accelerated their investment in self-driving technology research and development is that Tesla has combined EVs with self-driving technology, and has established an industry benchmark, to some extent. It will be difficult for other automakers to compete with Tesla if their EV products are not equipped with self-driving technology to improve the safety and comfort of EVs.

In the literature, numerous studies have aimed at taking action at congested spots to mitigate traffic jams. Researchers also have been paying attention to traffic management of mixed traffic systems containing both connected and automated vehicles (CAVs) and human-driven vehicles (HDVs). To the best of our knowledge, scant research work in the literature has tackled the joint problem of traffic congestion prevention, mixed traffic flow management, and route/charging planning for EVs. Accordingly, this work presents a novel traffic management scheme that integrates route/charging planning for EVs and urban traffic congestion control. A mixed traffic system that includes both CAVs and HDVs is considered in this work. Notably, to reduce the number of vehicles driving on the roads effectively, only CAV fleet vehicles are allowed to provide ride-sharing mobility-on-demand (MoD) services during peak periods, whereas traditional vehicle drivers can own either CAVs or HDVs.

An adaptive traffic control mechanism is applied to each expressway or to portions of busy local roads during peak periods. Here we adopt prerouting and rerouting reservation schemes to control traffic flow during rush hours. An EV is required to make a prerouting reservation before its departure. In the meantime, portions of traffic volumes on each road segments under traffic control during peak periods are reserved for the EVs that have already departed from their origins. In the case where some EVs do not arrive at certain road segments on time after making a reservation, this kind of reassignment mechanism can boost the traffic volumes on underutilized road segments during peak hours. In addition, no traffic control is applied to public transportation, so as to provide an incentive for the public to take public transportation to help mediate urban traffic congestion.

If an EV needs to recharge on the way to its destination due to a battery electricity shortage, three charging options, including plug-in charging stations [4], battery-swapping services [5], and on-road wireless charging [6], can be chosen according to a specific charging preference set by an EV driver. In contrast, the most convenient charging option is selected for the CAV fleet vehicles that are offering ridesharing MoD services before recharging. A series of simulations were conducted to examine the effectiveness of the proposed work. The simulation results reveal that the proposed mechanism can improve urban traffic flows during peak hours and meet the demands of EV users effectively.

The remainder of this paper is organized as follows. Section 2 gives a detailed description of the proposed mechanism. The simulation results and the conclusions are given in Sections 3 and 4, respectively.

2. RELATED WORK

In this section, we discuss on related work of this paper in three aspects, including the recent research progress about urban traffic control, mixed traffic flow management, and the route/charging planning of EVs.

In the recent literature, numerous studies are being conducted to develop solutions for improving the performance of urban traffic networks. To name a few, Artuñedo *et al.* proposed an algorithm for cooperative control of urban subsystems to provide a solution for mobility problems in urban areas [7]. The interconnected traffic lights controller network adapts traffic lights cycles, based on traffic and air pollution sensory information, in order to improve the performance of urban traffic networks. Godoy *et al.* conducted a driverless experiment consisted of a 100-km route around Madrid in Spain, including both urban and motorway environments [8]. A leading vehicle shares information about its route in real time. A trailing vehicle is able to follow the leader's trajectory using a combination of fuzzy logic controllers. Castaño *et al.* presented a self-tuning method to maximize the reliability of LiDAR sensors network for obstacle detection in the Internet of Things mobility scenarios [9]. The experimental results demonstrated that the self-tuning method is an appropriate strategy to increase the reliability of the sensor network while minimizing detection thresholds. Chu *et al.* proposed an advantage actor critic based multi-agent reinforcement learning algorithm for scalable adaptive traffic signal control in urban traffic networks [10]. A spatial discount factor was introduced to reduce the learning difficulty. Yao *et al.* proposed a dynamic predictive control framework for traffic signal control in a cross-sectional vehicle infrastructure integration environment [11]. Li *et al.* proposed a multi-agent reinforcement learning method to achieve optimal traffic control by enhancing the cooperation between traffic signals [12]. By introducing the knowledge-sharing enabled communication protocol, each agent can access to the collective representation of the traffic environment collected by all agents. Boukerche *et al.* employed reinforcement learning agents to cooperatively control the traffic signals by improving the reward and state representation based on the state-of-the-art max-pressure control theory [13]. A traffic state prediction method was proposed to address the data transmission delay issue by decreasing the discrepancy between the real-time and delayed traffic conditions. Mou developed a signal timing control model to optimize road capacity, delay time and the number of stops at the intersections, based on total signal cycle time, green light time and the maximum number of vehicles in each direction of intersection [14]. Liu *et al.* proposed a traffic flow control model to deal with the uncertainties in the turning ratio by using distributionally robust chance constraints [15]. The model allows one to compute the optimal control action that maximizes some objective, under all possible distributions of network parameters. Li *et al.* proposed a data augmented deep behavioral cloning method to imitate the problem-solving skills of traffic engineers [16]. Their method was under a conceptual parallel learning framework that incorporates machine learning techniques for solving decision-making problems in complex systems. You *et al.* employed a stochastic Markov decision process to model the stochastic behaviors of the vehicles in highway traffic [17]. The state of their model is dynamically modified based on the complicated traffic information.

In recent years, researchers started to focus on traffic management of mixed traffic systems containing both CAVs and HDVs. To name a few, Du *et al.* proposed a coupled vehicle-signal control method to optimize the traffic signal timing and driving trajectories of

CAVs [18]. The signal timing is continuously optimized to minimize the total delay at the intersection. CAVs generate eco-driving trajectories using the received signal timing information and the planned arrival time to reduce fuel consumption. Feng *et al.* proposed a robust platoon control framework for mixed traffic flow based on tube model predictive control (MPC) [19]. The prediction uncertainty is dynamically mitigated by the feedback control and restricted inside a set with a high probability. Bahrami and Roorda formulated the multi-class traffic assignment problem as a nonlinear complementarity problem to find optimal traffic management policies [20]. Zheng *et al.* proposed a stochastic model for mixed traffic flow [21]. They used the proposed model to investigate the interaction between CAVs and HDVs. Li *et al.* proposed a theoretical model to demonstrate that road capacity can be increased with proper Right-of-Way reallocation for the mixed flow [22]. Kamal *et al.* presented an adaptive traffic signal control scheme for mixed traffic scenario at a road intersection [23]. The traffic signals are optimized to minimize the total crossing time of all vehicles. Qi *et al.* analyzed the mixed traffic dynamics of CAVs and HDVs, and derived the arrival–departure curves relationship using a combination of Newell car-following and Akçelik acceleration model [24]. Yang *et al.* proposed a hierarchical and cooperative driving framework for mixed traffic flow on urban arterials [25]. The proposed framework combined centralized and distributed control concepts, where the infrastructure generates optimal signal timing plans and provided high-level trajectory guidance to the CAVs while detailed trajectories are generated by each vehicle. Sharma *et al.* utilized intelligent driver model (IDM) with estimation errors to model HDVs since it incorporates human factors such as estimation errors [26]. Connected vehicle driving strategy integrated with IDM was utilized to model CAVs because it incorporates driver compliance, which is a critical human factor for the success of CAVs. Guo and Jia proposed an inverse MPC-based approach to model and predict the longitudinal behaviors of HDVs in connected mixed traffic environments [27]. Its predictions can be utilized by the MPC of following CAVs for improved control accuracy, riding comfort, and energy efficiency. Wu *et al.* developed a distributed control framework for the cooperative control of mixed urban and freeway traffic networks [28]. A MPC strategy was applied to optimize the traffic signals in the urban network and the variable speed limits in the freeway network. Ngoduy *et al.* proposed a dynamic system optimum formulation for the multi-class dynamic traffic assignment (DTA) problem of fixed traffic flow [29]. The proposed method used the concept of link based approach to develop a multi-class DTA model that equally distributes the total physical queues over the links while considering explicitly the variations in capacity and backward wave speeds due to class proportions. Wang *et al.* proposed a multi-class traffic assignment problem with elastic demand to estimate the impacts of link tolls on equilibrium flows [30]. It not only enhances behavioral realism for modeling the route choices of HDV and CAV travelers by considering their knowledge level of traffic conditions but also captures the elasticity of both HDV and CAV demand in response to link toll rates.

In addition to the urban traffic management problem, the route/charging planning of EVs has attracted researchers' attention in recent years due to deteriorated urban air quality. To name a few, Zhang *et al.* proposed a charging guidance strategy for urgent charging EVs to fast charging stations based on the virtual service range [31]. Ammous *et al.* proposed formulated a joint problem of minimizing the average trip time for an EV and the average cost of charging as a dual-objective convex optimization problem [32]. Moradipari and Alizadeh designed optimal pricing and routing schemes for the setting that users choose their priority level and energy request amount from the differentiated service offered by EV public charging stations owned by a charging network operator [33]. An EV routing problem with time windows was investigated in [34] through integrating decisions on two charging options of partial recharging and battery swapping. A mixed integer programming model was developed to solve the optimization problem. Qian *et al.* proposed a deep reinforcement learning-based EV charging navigation that minimizes the total travel time and the charging cost at charging stations [35]. They formulated EV charging navigation as a Markov Decision Process with an unknown transition probability. Chen *et al.* proposed a bi-level mathematical model to derive optimal design that minimize the joint cost of facility constructions and EV drivers' travel and waiting time over the network [36]. Basso *et al.* proposed a probabilistic energy consumption model with machine learning that can estimate the expected energy and variance for the road links, paths, and routes [37]. A two-stage routing model that incorporates energy prediction and plans partial recharging using chance constraints was presented to provide reliable routing of EVs. Chakraborty *et al.* proposed a heuristic to ensure that the EVs can always route through a path that minimizes the energy consumption and the total time to travel [38]. A multi-objective optimization problem considering real-world specifications and constraints was formulated and a graph-based multi-objective heuristic algorithm was proposed to obtain the desired solutions quickly. Bac and Erdem proposed a framework of EV routing problem with time windows [39]. Partial recharging was considered in the framework with the multiple depots and heterogeneous fleet structure under real-life constraints such as multiple customer visits.

3. URBAN TRAFFIC CONTROL MECHANISM FOR MIXED TRAFFIC FLOW

In this work, all road segments in the whole metropolitan area are managed by an urban traffic control center. The traffic flow at each road segment under traffic control is divided into two categories: one is for EVs reserving their routes before departure and the other is for the EVs that are on the way to their destination. As shown in the middle-left of Figure 1, a prerouting module is used by an EV user to select and reserve the most appropriate candidate route for an EV from its origin to the destination. This is done before departure based on the historical traffic data. In the case of a possible electricity shortage of the EV battery during the trip, this module determines the route and charging point based on the preset priority. Notably, support vector regressions (SVRs) are applied to compute the charging time at each charging point, and the traverse time of an EV at each road segment/intersection, based on the historical traffic data. The SVR method was chosen because it has been proven to predict traffic flows with a high degree of accuracy and to perform traffic data analysis well in the literature [40].

Once the EV prerouting module computes the most appropriate route from the origin to the destination that fits the preset preference of an EV, the module then sends reservation requests for the road segments on the route to the urban traffic control center. Since deviations between the prediction computed by SVRs and the real-time traffic and charging conditions might be significant enough to affect the real-time urban traffic condition, especially during rush hours, a real-time congestion control module, as shown on the right of Figure 1, is adopted by the urban traffic control center to deal with the volatile traffic conditions. Road segment reservation and cancellation requests from EVs are updated at the urban traffic control center during a fixed short interval, which can be dynamically adjusted by the urban traffic management control center during peak periods.

At the end of the preset short interval, the urban traffic control center sorts the road segment reservation request queues and determines whether an EV is allowed to drive on designated road segments during rush hours. In case of no route being available due to traffic control policies, the EVs that are declined permission to drive on some popular routes then turn to finding another less-saturated route to their destination. Notably, the ratios of approvals for the road segment reservations of EVs that carry one, two, or more passengers can be set up dynamically for different expressways and local roads during peak periods. In addition, the local roads that are less saturated are not subject to traffic control in order that the entire urban area can be connected, and late-booking EVs that are denied permission to drive on popular expressways and local roads are still capable of reaching their destinations during peak periods.

In addition to the prerouting module mentioned above, this work allows a moving EV to employ the real-time rerouting module (as shown in the bottom-left of Figure 1) to find a better route that fits the demand of the EV. Each moving EV regularly checks whether the arrival time at each road intersection on the route is earlier than or delayed from the originally estimated time. If so, the reroute process will be activated to find a less-congested route to the destination, as this work reserves a proportion of traffic volumes for real-time driving EVs. The ratio of the prerouting EVs to the real-time rerouting ones at a road segment can be adjusted for different expressways and local roads. Meanwhile, this work only allows CAVs to drive on expressways during peak hours to ensure smooth traffic flow on expressways in the urban area.

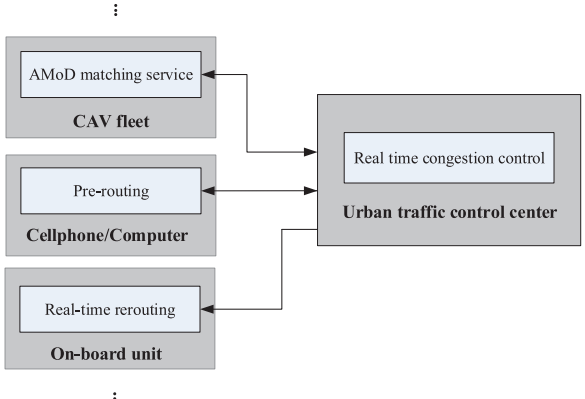

Figure 1 | Architecture of urban traffic control mechanism for mixed traffic flow.

As shown in the top-left of Figure 1, in the case of there being no satisfactory route due to traffic congestion in the urban area, the EV users will request rideshare service from an autonomous mobility-on-demand (AMoD) fleet. If no rideshare service suits a passenger's need, scheduled information about public transportation is suggested as an alternative means of transportation.

A brief flow chart of the proposed urban traffic control mechanism for mixed traffic flow is illustrated in Figure 2. The detailed descriptions of the above-mentioned modules are given below.

3.1. Prerouting of an EV

This module is used to set up the route of an EV before its departure. The updated traffic information can be downloaded to any cellphone or computer that is running the module. The road map of the urban area is expressed as a directed graph. Each node of the directed graph stands for the position of a road intersection. During the route computation, the EV checks whether the capacity of its battery, denoted as the state of charge (SOC), is sufficient to arrive at the destination without depleting the electricity of the battery. The battery charging option that suits the need of the EV is arranged in this module if recharging is required before the EV reaches the destination.

This work assumes three charging options, including plug-in charging, battery-swapping, or on-roads wireless charging, which can be chosen to fit the need of an EV. The option of on-road wireless charging would be the most popular during rush periods, especially for the AMoD fleets. However, while a CAV in an AMoD fleet is off duty, a plug-in charging option might suit its need. This latter option also fits the preference of an EV owner while she/he stays at work/home for some period of time. Before the prerouting is initiated, the EV will request the updated traffic and charging information from the urban traffic control center. This work also assumes real-time electricity charging prices are regularly updated by the charging stations/services.

Accordingly, a route that suits the demand of an EV can be obtained by

$$\begin{aligned}\text{Min}\ \Bigg\{ & \omega_1 \cdot rl + \omega_2 \cdot \left(rt_{c_{dt}} - rt_{c_1}\right) + \omega_3 \cdot \Bigg[\sum_{1 \le i < dt} \phi_{pcs_{c_i,p_j}} \\ & \cdot RCP_{pcs_{c_i,p_j}}\left(rt_{c_i}\right) \cdot cp_{pcs_{c_i,p_j}} \cdot ct_{pcs_{c_i,p_j}} + \sum_{1 \le i < dt} \theta_{wcs_{c_i,c_{i+1}}} \\ & \cdot RCP_{wcs_{c_i,c_{i+1}}}\left(rt_{c_i}\right) \cdot cp_{wcs_{c_i,c_{i+1}}} \cdot SD_{c_i,c_{i+1}}\left(rt_{c_i}\right) \\ & + \sum_{1 \le i < dt} \psi_{bss_{c_i,p_k}} \cdot RCP_{bss_{c_i,p_k}}\left(rt_{c_i}\right) \cdot \left(SOC^{max} - SOC_{c_i}\right) \Bigg] \Bigg\} \end{aligned} \tag{1}$$

subject to

$$rl = \sum_{\substack{0 \le r < \varsigma \\ pd_0 = 1 \\ pd_\varsigma = dt}} \left(\sum_{pd_r \le i < pd_{r+1}} sl_{c_i,c_{i+1}} \right) \tag{2}$$

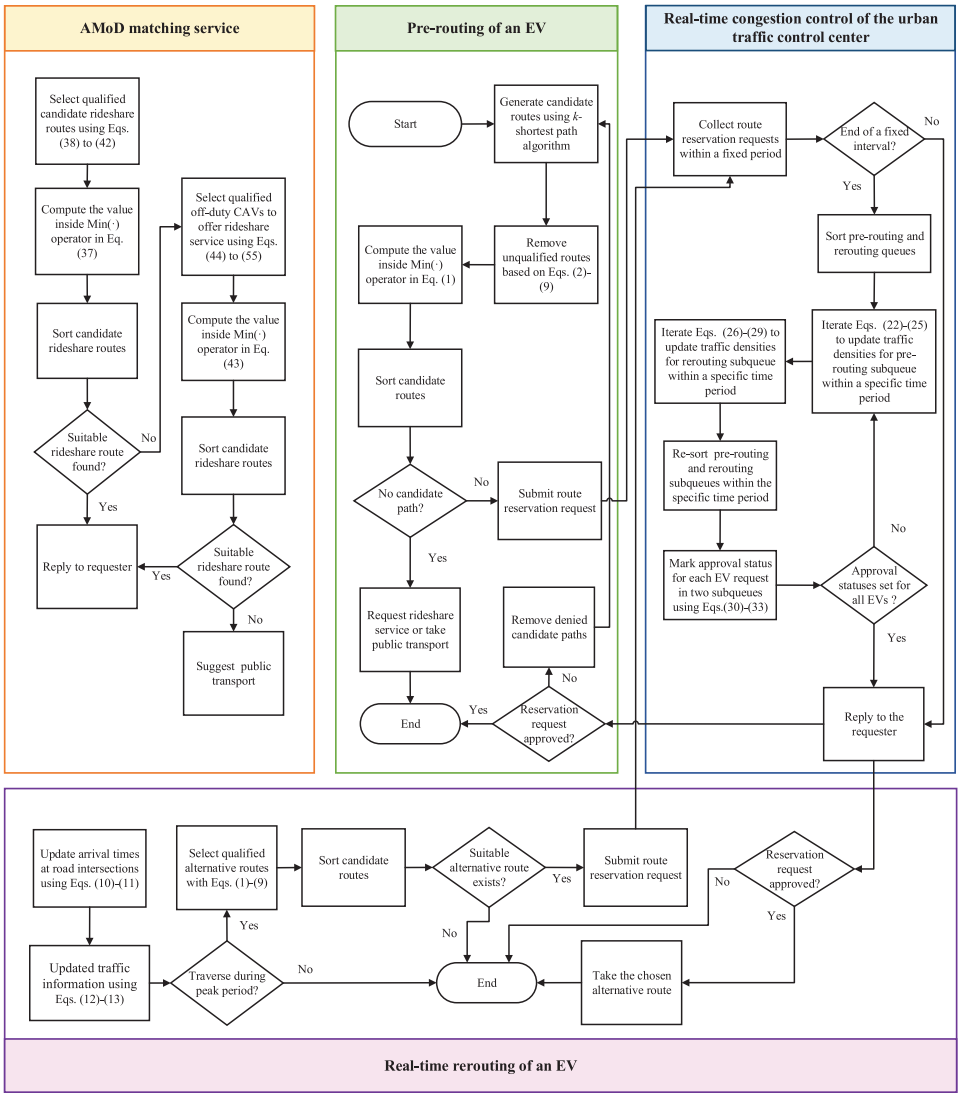

Figure 2 | Flow chart of the proposed urban traffic control mechanism for mixed traffic flow.

$$
\begin{aligned}
&rt_{c_{i+1}} \\
&= rt_{c_i} + ID_{c_i,c_{i+1}}\left(rt_{c_i}\right) + \left(1-\phi_{pcs_{c_i,p_j}}\right) \\
&\cdot \left(1-\psi_{bss_{c_i,p_j}}\right)\cdot SD_{c_i,c_{i+1}}\left(rt_{c_i}\right) + \phi_{pcs_{c_i,p_j}} \\
&\cdot \left[ct_{pcs_{c_i,p_j}} + SD_{c_i,p_j}\left(rt_{c_i}\right) + SD_{p_j,c_{i+1}}\left(rt_{c_i} + SD_{c_i,p_j}\left(rt_{c_i}\right)\right)\right] \\
&+ \psi_{bss_{c_i,p_k}}\cdot \left[BSD_{bss_{c_i,p_k}}\left(rt_{c_i}\right) + SD_{c_i,p_k}\left(rt_{c_i}\right)\right. \\
&\left. + SD_{p_k,c_{i+1}}\left(rt_{c_i} + SD_{c_i,p_k}\left(rt_{c_i}\right)\right)\right],\ 1 \le i < dt
\end{aligned} \tag{3}
$$

$$
\rho^{pr}_{c_i,c_{i+1},np}\left(rt_{c_i}\right) < \kappa\left(rt_{c_i}\right)\cdot \rho^{pr,max}_{c_i,c_{i+1},np}\left(rt_{c_i}\right),\ 1 \le np \le 3 \tag{4}
$$

$$
\begin{aligned}
SoC_{c_{i+1}} &= SoC_{c_i} + \eta\cdot\phi_{pcs_{c_i,p_j}}\cdot cp_{pcs_{c_i,p_j}}\cdot ct_{pcs_{c_i,p_j}} + \eta \\
&\cdot \theta_{wcs_{c_i,c_{i+1}}}\cdot cp_{wcs_{c_i,c_{i+1}}}\cdot SD_{c_i,c_{i+1}}\left(rt_{c_i}\right) + \psi_{bss_{c_i,p_k}} \\
&\cdot \left(SOC^{max} - SoC_{c_i}\right) - ap\cdot sl_{c_i,c_{i+1}},\ 1 \le i < dt
\end{aligned} \tag{5}
$$

$$
0 \le ct_{pcs_{c_i,p_j}} \le ct^{max}_{pcs_{c_i,p_j}},\ \text{if}\,\phi_{pcs_{c_i,p_j}} = 1 \tag{6}
$$

$$
SOC^{min} \le SoC_{c_i} \le SOC^{max},\ 1 \le i \le dt \tag{7}
$$

$$
\sum_{1\le i<dt}\left(\phi_{pcs_{c_i,p_j}} + \theta_{wcs_{c_i,c_{i+1}}} + \psi_{bss_{c_i,p_k}}\right) \ge 1, \text{if}\, SOC^{org} - ap\cdot rl < SOC^{min} \tag{8}
$$

$$
0 \le \eta \le 1 \tag{9}
$$

where the definitions of the parameters used in the above equations are given below:

(i) Three parameters used in Eq. (1) from left to right stand for the total route length, the total traveling time, and the charging costs, respectively. Three weights ω_1, ω_2, and ω_3 are

used to indicate the significance of the each minimization objective. ω_3 is set to zero if battery electricity is sufficient for the EV to arrive at its destination.

(ii) c_1 and c_{dt} represent the origin and the destination, respectively. rl denotes the total route distance, and $sl_{c_i,c_{i+1}}$ denotes the road segment length connecting c_i and c_{i+1}. rt_{c_i} is the time that the EV arrives at the road intersection c_i. This module assumes there are ς pickup/drop-off points on the route, and pd_r represents the index of the road intersection where the EV stops at the pickup/drop-off points. Here pd_0 and pd_ς denote the origin and the destination, respectively.

(iii) $SD_{c_i,c_{i+1}}(t)$ stands for the travel time of the vehicle traversing the road segment that connects c_i and c_{i+1} at time t, whereas $ID_{c_i,c_{i+1}}(t)$ represents the traverse time of the EV that goes through the road intersection c_i before entering the road segment that connects c_i and c_{i+1} at time t. Here we assume that $ID_{c_i,c_{i+1}}(t)$ and $SD_{c_i,c_{i+1}}(\cdot)$ are predicted by using SVRs, and their values are kept at the database of the urban traffic control center.

(iv) SOC^{max} denotes the full battery capacity, SoC_{c_i} represents the SOC of the battery when the EV reaches c_i, whereas SOC^{min} is the minimal capacity of the battery. $wcs_{c_i,c_{i+1}}$ denotes the wireless charging service on the road segment between c_i and c_{i+1}, whereas bss_{c_i,p_k} and pcs_{c_i,p_j} represent the battery-swapping service and the plug-in charging station that are close to or located at road intersection c_i, respectively. $\phi_{pcs_{c_i,p_j}}$, $\theta_{wcs_{c_i,c_{i+1}}}$, and $\psi_{bss_{c_i,p_k}}$ are binary decision variables that indicate whether pcs_{c_i,p_j}, $wcs_{c_i,c_{i+1}}$, and bss_{c_i,p_k} are chosen for battery charging for the EV, respectively.

(v) $RCP_q(t)$ represents the real-time charging electricity price at charging point q at time t. $cp_{pcs_{c_i,p_j}}$ and $cp_{wcs_{c_i,c_{i+1}}}$ stand for the charging electricity per second for the on-road wireless charging, $wcs_{c_i,c_{i+1}}$, and the plug-in charging station, pcs_{c_i,p_j}, respectively. $ct^{max}_{pcs_{c_i,p_j}}$ and $ct_{pcs_{c_i,p_j}}$ stand for the upper limit of charging time and the actual charging time of the EV at the plug-in charging station pcs_{c_i,p_j}, respectively. Notably, this work assumes the EV is kept charged with an on-road wireless charging service while it moves along the whole road segment. Thus, the traverse time $SD_{c_i,c_{i+1}}(t)$ is equal to the charging time of an on-road wireless charging service. $BSD_{bss_{c_i,p_k}}(t)$ stands for the battery-swapping time of bss_{c_i,p_k} at time t. Here, it should be noted that $BSD_{bss_{c_i,p_k}}(\cdot)$ is predicted by using SVRs, and the values of $BSD_{bss_{c_i,p_k}}(\cdot)$ along with $ct^{max}_{pcs_{c_i,p_j}}$ are kept at the database of the urban traffic control center. Meanwhile, all charging points continually report the real-time charging prices to the urban traffic control center during a preset fixed short interval.

(vi) $\kappa(rt_{c_i})$ denotes a binary flag that indicates whether a HDV is allowed to drive on an expressway during peak periods. In the case where the EV is a HDV, and HDVs are not allowed to drive on the road segment during peak periods, $\kappa(rt_{c_i})$ is set to zero when rt_{c_i} falls within a peak period. $\rho^{pr}_{c_i,c_{i+1},np}(t)$ and $\rho^{pr,max}_{c_i,c_{i+1},np}(t)$ denote the updated traffic density of the road segment that connects c_i and $c_{j,i+1}$ for the permitted prerouting traffic flow traffic flow of EVs that carry np passengers, and the threshold of the traffic density for the permitted prerouting traffic flow of EVs that carry np passengers, at time t, respectively. ap is the electricity consumption of the EV battery per kilometer. Notably, $\rho^{pr,max}_{c_i,c_{i+1},np}(t)$ is set to infinity if the road segment between c_i and c_{i+1} is free from traffic control at time t.

The three optimization objectives to be achieved in Eq. (1), from left to right, stand for the total route length, the total traveling time, and the charging cost, respectively. Each coefficient of the three optimization objectives presents the weight of the corresponding preference set by the EV user. As shown in the top-center of Figure 2, we first employ the well-known k-shortest path algorithm [41] to generate at most k- shortest candidate routes in real time. Then the candidate routes that exceed the preset deadline to reach the destination are removed from the list in accordance with the list of constraints given in Eqs. (2–9). Next, we derive the value inside the Min$(\cdot)$ operator in Eq. (1) for each qualified candidate route by computing the inner product of the three weights and the corresponding objectives. The candidate routes are then sorted in ascending order, based on the computation result obtained above.

After the most appropriate route is derived from the abovementioned equations, a route reservation request is submitted to the urban traffic control center. The EV confirms with the urban traffic control center whether the road segment reservation requests are all approved. In the case where any of the road segments that the EV attempts to reserve is declined, the EV rules out all at-capacity road segments and looks for an alternative route that is less congested.

The prerouting process iterates until the route is found. In the case where the travel time is much longer than expected due to traffic congestion, the alternative of a rideshare or public transport is suggested to the EV user.

3.2. Real-Time Rerouting of an EV

As mentioned above, some EVs might be absent from the designated road intersections at the expected arrival times after making route reservations, or their arrival times might be earlier than or delayed from the originally estimated times due to fluctuating traffic conditions. Accordingly, this module is executed at an EV's on-board unit (OBU) at every fixed interval, set as five minutes or fewer, to deal with the abovementioned unexpected situations after an EV starts moving. As shown in the bottom of Figure 2, this module first receives updated traffic information from the urban traffic control center and checks whether the time for an EV arriving at each road intersection on the route is shifted from an off-peak period to a peak period:

$$rt'_{c_1} = rt_{c_1} \tag{10}$$

$$
\begin{aligned}
rt'_{c_{i+1}} = {} & rt'_{c_i} + ID_{c_i,c_{i+1}}\left(rt'_{c_i}\right) + \left(1-\phi_{pcs_{c_i,p_j}}\right)\cdot\left(1-\psi_{bss_{c_i,p_j}}\right) \\
& \cdot SD_{c_i,c_{i+1}}\left(rt'_{c_i}\right) + \phi_{pcs_{c_i,p_j}}\cdot\left[ct_{pcs_{c_i,p_j}}\right. \\
& \left. + SD_{c_i,p_j}\left(rt'_{c_i}\right) + SD_{p_j,c_{i+1}}\left(rt'_{c_i} + SD_{c_i,p_j}\left(rt'_{c_i}\right)\right)\right] \\
& + \psi_{bss_{c_i,p_k}}\cdot\left[BSD_{bss_{c_i,p_k}}\left(rt'_{c_i}\right) + SD_{c_i,p_k}\left(rt'_{c_i}\right)\right. \\
& \left. + SD_{p_k,c_{i+1}}\left(rt'_{c_i} + SD_{c_i,p_k}\left(rt'_{c_i}\right)\right)\right],\ 1 \le i < v
\end{aligned} \tag{11}
$$

$$
cm_{c_i,c_{i+1}} = \begin{cases} 1, & \text{if } \rho^{rr}_{c_i,c_{i+1},np}\left(rt_{c_i}\right) < \rho^{rr,max}_{c_i,c_{i+1},np}\left(rt_{c_i}\right) \text{ and} \\ & \rho^{rr,max}_{c_i,c_{i+1},np}\left(rt'_{c_i}\right) \le \rho^{rr}_{c_i,c_{i+1},np}\left(rt'_{c_i}\right) \\ 0, & \text{Otherwise} \end{cases} \tag{12}
$$

$$
ri = \sum_{i=1}^{v-1} cm_{c_i,c_{i+1}} \tag{13}
$$

where c_1 and c_v denote the indices of the approaching road intersection and the destination, respectively. rt'_{c_i} represents the updated arrival timestamp at the road intersection c_i, v is the updated index node for the destination. $\rho^{rr}_{c_i,c_{i+1},np}(t)$ and $\rho^{rr,max}_{c_i,c_{i+1},np}(t)$ stand for the updated traffic density for the admitted rerouting traffic flow of EVs that carry np passengers and the permitted traffic density of the admitted rerouting traffic flow of EVs that carry *np* passengers, set for the road segment connecting c_i and c_{i+1} at time t, respectively.

Eq. (12) examines whether the estimated arrival time at c_i is shifted from an off-peak period to a peak period. This situation must be dealt with to prevent any possible traffic congestion from increasing traffic volumes during rush hours. As a result, this module executes Eqs. (1–9) again to look for an alternative route if $ri > 0$. Notably, at this moment, $\rho^{pr}_{c_i,c_{i+1},np}\left(rt_{c_i}\right)$ and $\rho^{pr,max}_{c_i,c_{i+1},np}\left(rt_{c_i}\right)$ in Eq. (4) should be replaced by the corresponding $\rho^{rr}_{c_i,c_{i+1},np}\left(rt'_{c_i}\right)$ and $\rho^{rr,max}_{c_i,c_{i+1},np}\left(rt'_{c_i}\right)$, respectively.

3.3. Real-Time Congestion Control of the Urban Traffic Control Center

Within a fixed short interval, which can be dynamically tuned during peak periods and off-peak periods, the urban traffic control center keeps track of prerouting and rerouting road segment reservation and cancellation requests. The prerouting and rerouting reservation queues for each road segment are then resorted, in ascending order, based on the updated arrival times of EVs at the end of each fixed interval. The attributes of the two reservation queues for each road segment under traffic control include the arrival timestamp of each incoming EV, the number of passengers carried by the EV, the time that the EV issued the reservation request, the traffic density at the arrival time of the EV, and the approval status of the EV.

As shown in the right of Figure 2, after the two queues are resorted, this module initializes the variables needed during the computation of the traffic density of the road segment between l and m:

$$
u^s_{l,m} = 1 \tag{14}
$$

$$
\tau_{l,m} = \mathbf{PRQ}_{l,m}[1].arr \tag{15}
$$

$$
\mu^s_{l,m} = 1 \tag{16}
$$

$$
\sigma_{l,m} = \mathbf{RRQ}_{l,m}[1].arr \tag{17}
$$

where $\mathbf{PRQ}_{l,m}$ and $\mathbf{RRQ}_{l,m}$ stand for the prerouting and rerouting reservation requests, sorted by the arrival times of the EVs over the road segment connecting l and m, respectively. $\tau_{l,m}$ and $\sigma_{l,m}$ stand for the arrival times of the EVs in the sorted prerouting and rerouting reservation queues for the road segment connecting l and m, respectively. Here $\mathbf{PRQ}_{l,m}[\cdot].arr$ and $\mathbf{RRQ}_{l,m}[\cdot].arr$ represent the attribute of each EV's arrival time in the prerouting and rerouting queues, respectively. $u^s_{l,m}$ and $\mu^s_{l,m}$ represent the starting indices of the sorted prerouting and rerouting reservation queues for the road segment connecting l and m at time $\tau_{l,m}$ and $\sigma_{l,m}$, respectively.

As mentioned earlier, the granting of a road segment reservation for an EV depends upon the number of passengers in the EV. The approval ratios for the road segment reservations of EVs with one, two, or more passengers are adjusted dynamically during peak periods. Based on the arrival times of EVs, the traffic densities of prerouting and rerouting traffic flows with different numbers of EV passengers can be computed by

$$
u^c_{l,m} = u^s_{l,m} \tag{18}
$$

$$
\mu^c_{l,m} = \mu^s_{l,m} \tag{19}
$$

$$
\lambda^{pr}_{l,m,1}\left(\tau_{l,m}\right) = \lambda^{pr}_{l,m,2}\left(\tau_{l,m}\right) = \lambda^{pr}_{l,m,3}\left(\tau_{l,m}\right) = 0 \tag{20}
$$

$$
\lambda^{rr}_{l,m,1}\left(\sigma_{l,m}\right) = \lambda^{rr}_{l,m,2}\left(\sigma_{l,m}\right) = \lambda^{rr}_{l,m,3}\left(\sigma_{l,m}\right) = 0 \tag{21}
$$

$$
\arg_{u^e_{l,m}}\left(\mathbf{PRQ}_{l,m}\left[u^e_{l,m}\right].arr < {}_{l,m} + 1 \le \mathbf{PRQ}_{l,m}\left[u^e_{l,m}+1\right].arr\right) \tag{22}
$$

$$
\begin{aligned}
& \rho^{pr}_{l,m,\mathbf{PRQ}_{l,m}\left[u^c_{l,m}\right].np}\left(\tau_{l,m}\right) \\
& = \min\left(\rho^{pr}_{l,m,\mathbf{PRQ}_{l,m}\left[u^c_{l,m}\right].np}\left(\tau_{l,m}\right) + 1, \rho^{pr,max}_{l,m,\mathbf{PRQ}_{l,m}\left[u^c_{l,m}\right].np}\left(\tau_{l,m}\right)\right)
\end{aligned} \tag{23}
$$

$$
\lambda^{pr}_{l,m,\mathbf{PRQ}_{l,m}\left[u^c_{l,m}\right].np}\left(\tau_{l,m}\right) = \lambda^{pr}_{l,m,\mathbf{PRQ}_{l,m}\left[u^c_{l,m}\right].np}\left(\tau_{l,m}\right) + 1 \tag{24}
$$

$$
u^c_{l,m} = u^c_{l,m} + 1 \tag{25}
$$

$$\arg\underset{\mu^e_{l,m}}{}\left(\mathbf{RRQ}_{l,m}\left[\mu^e_{l,m}\right].arr < \sigma_{l,m}+1 \le \mathbf{RRQ}_{l,m}\left[\mu^e_{l,m}+1\right].arr\right) \tag{26}$$

$$\rho^{rr}_{l,m,\mathbf{RRQ}_{l,m}\left[\mu^c_{l,m}\right].np}\left(\sigma_{l,m}\right) = \min\left(\rho^{rr}_{l,m,\mathbf{RRQ}_{l,m}\left[\mu^c_{l,m}\right].np}\left(\sigma_{l,m}\right)+1, \rho^{rr,max}_{l,m,\mathbf{RRQ}_{l,m}\left[\mu^c_{l,m}\right].np}\left(\sigma_{l,m}\right)\right) \tag{27}$$

$$\lambda^{rr}_{l,m,\mathbf{RRQ}_{l,m}\left[\mu^c_{l,m}\right].np}\left(\sigma_{l,m}\right) = \lambda^{rr}_{l,m,\mathbf{RRQ}_{l,m}\left[\mu^c_{l,m}\right].np}\left(\sigma_{l,m}\right)+1 \tag{28}$$

$$\mu^c_{l,m} = \mu^c_{l,m}+1 \tag{29}$$

where $u^c_{l,m}$ and $u^e_{l,m}$ represent the current index and the last index of the sub-queue of $\mathbf{PRQ}_{l,m}$ with the arrival times of EVs at the road segment connecting l and m falling within the period of $[\tau_{l,m}, \tau_{l,m}+1)$, whereas $\mu^c_{l,m}$ and $\mu^e_{l,m}$ respectively stand for the current index and the last index of the sub-queue of $\mathbf{RRQ}_{l,m}$ with the arrival times of EVs falling within $[\sigma_{l,m}, \sigma_{l,m}+1)$. Meanwhile, $\lambda^{pr}_{l,m,np}\left(_{l,m}\right)$ and $\lambda^{rr}_{l,m,np}\left(\sigma_{l,m}\right)$ stand for the number of the EVs that carry np passengers within the intervals $[\tau_{l,m}, \tau_{l,m}+1)$ and $[\sigma_{l,m}, \sigma_{l,m}+1)$, respectively. The attributes $\mathbf{PRQ}_{l,m}[\cdot].np$ and $\mathbf{RRQ}_{l,m}[\cdot].np$ denote the number of passengers carried by the EV in $\mathbf{PRQ}_{l,m}$ and $\mathbf{RRQ}_{l,m}$, respectively. $\rho^{pr}_{l,m,\mathbf{PRQ}_{l,m}\left[u^c_{l,m}\right].np}\left(\tau_{l,m}\right)$ and $\rho^{rr}_{l,m,\mathbf{RRQ}_{l,m}\left[\mu^c_{l,m}\right].np}\left(\sigma_{l,m}\right)$ stand for the current traffic densities of the traffic flows of the EVs that carry $\mathbf{PRQ}_{l,m}\left[u^c_{l,m}\right].np$ and $\mathbf{RRQ}_{l,m}\left[\mu^c_{l,m}\right].np$ passengers within the period $[\tau_{l,m}, \tau_{l,m}+1)$ and $[\sigma_{l,m}, \sigma_{l,m}+1)$, respectively; whereas $\rho^{pr,max}_{l,m,\mathbf{PRQ}_{l,m}\left[u^c_{l,m}\right].np}\left(\tau_{l,m}\right)$ and $\rho^{rr,max}_{l,m,\mathbf{RRQ}_{l,m}\left[\mu^c_{l,m}\right].np}\left(\sigma_{l,m}\right)$ denote the permitted traffic densities set for the prerouting and rerouting requests with the traffic flow of the corresponding number of passengers within $[\tau_{l,m}, \tau_{l,m}+1)$ and $[\sigma_{l,m}, \sigma_{l,m}+1)$, respectively.

Eqs. (22–25) are iterated until $u^c_{l,m} > u^e_{l,m}$, and Eqs. (26–29) are iterated until $\mu^c_{l,m} > \mu^e_{l,m}$. At this moment, the traffic densities for the pre-routing and rerouting requests with the traffic flow of the corresponding number of passengers within $[\tau_{l,m}, \tau_{l,m}+1)$ and $[\sigma_{l,m}, \sigma_{l,m}+1)$ are derived.

Next, this module determines whether the EVs in the two queues are granted permission to enter the road segment connecting l and m within $[\tau_{l,m}, \tau_{l,m}+1)$ and $[\sigma_{l,m}, \sigma_{l,m}+1)$. The $\left(u^e_{l,m}-u^s_{l,m}+1\right)$ and $\left(\mu^e_{l,m}-\mu^s_{l,m}+1\right)$ elements at the prerouting and rerouting queues with the traffic flow of the corresponding number of passengers within $[\tau_{l,m}, \tau_{l,m}+1)$ and $[\sigma_{l,m}, \sigma_{l,m}+1)$ are resorted based on the order in which the EVs issued the prerouting and rerouting requests, respectively.

The settings of traffic density approval statuses for the $\left(u^e_{l,m}-u^s_{l,m}+1\right)$ prerouting requests and $\left(\mu^e_{l,m}-\mu^s_{l,m}+1\right)$ rerouting requests during the interval $[\tau_{l,m}, \tau_{l,m}+1)$ and $[\sigma_{l,m}, \sigma_{l,m}+1)$ can be expressed by

$$\mathbf{PRQ}_{l,m}\left[\mathbf{APR}^{\tau_{l,m}}_{np}\left[\zeta\right]\right].as = \begin{cases} 1, & \text{if } 1 \le \zeta \le \rho^{pr,max}_{l,m,\mathbf{PRQ}_{l,m}\left[u^c_{l,m}\right].np}\left(\tau_{l,m}\right) \\ 0, & \text{otherwise} \end{cases} \tag{30}$$

$$\mathbf{PRQ}_{l,m}\left[\mathbf{ARR}^{\tau_{l,m}}_{np}\left[\xi'\right]\right].td = \rho^{pr}_{l,m,\mathbf{PRQ}_{l,m}\left[\mu^c_{l,m}\right].np}\left(\tau_{l,m}\right),\ 1 \le \xi' \le \lambda^{pr}_{l,m,\mathbf{PRQ}_{l,m}\left[\mu^c_{l,m}\right].np}\left(\tau_{l,m}\right) \tag{31}$$

$$\mathbf{RRQ}_{l,m}\left[\mathbf{ARR}^{\sigma_{l,m}}_{np}\left[\xi\right]\right].as = \begin{cases} 1, & \text{if } 1 \le \xi \le \rho^{rr,max}_{l,m,\mathbf{RRQ}_{l,m}\left[\mu^c_{l,m}\right].np}\left(\sigma_{l,m}\right) \\ 0, & \text{otherwise} \end{cases} \tag{32}$$

$$\mathbf{RRQ}_{l,m}\left[\mathbf{ARR}^{\sigma_{l,m}}_{np}\left[\xi'\right]\right].td = \rho^{rr}_{l,m,\mathbf{RRQ}_{l,m}\left[\mu^c_{l,m}\right].np}\left(\sigma_{l,m}\right),\ 1 \le \xi' \le \lambda^{pr}_{l,m,\mathbf{RRQ}_{l,m}\left[\mu^c_{l,m}\right].np}\left(\sigma_{l,m}\right) \tag{33}$$

where $\mathbf{APR}^{\tau_{l,m}}_{np}$ and $\mathbf{ARR}^{\sigma_{l,m}}_{np}$ denote the sorted prerouting and rerouting sub-queues with np passengers based on the order in which the EVs issued the requests during $[\tau_{l,m}, \tau_{l,m}+1)$ and $[\sigma_{l,m}, \sigma_{l,m}+1)$, respectively. Notably, each record of $\mathbf{APR}^{\tau_{l,m}}_{np}$ and the record of $\mathbf{ARR}^{\sigma_{l,m}}_{np}$ are mapped into the original indices of the requesting EVs in $\mathbf{PRQ}_{l,m}$ and $\mathbf{RRQ}_{l,m}$, respectively. The attributes of $\mathbf{PRQ}_{l,m}[\cdot].as$ and $\mathbf{PRQ}_{l,m}[\cdot].td$ represent the approval status of the requesting EV and the traffic density of the traffic flow with the corresponding number of passengers carried by the EV, respectively; whereas $\mathbf{RRQ}_{l,m}[\cdot].as$ and $\mathbf{RRQ}_{l,m}[\cdot].td$ represent the corresponding attributes in the rerouting queue. Here, $\mathbf{PRQ}_{l,m}[\cdot].as$ is set to one if the prerouting reservation request of the corresponding EV is approved. Otherwise, it is set to zero. In other words, no more prerouting reservation requests for an EV with np passengers will be granted if the traffic density of the traffic flows with the corresponding number of passengers carried by the EV in the prerouting reservation reaches an upper bound. $\mathbf{RRQ}_{l,m}[\cdot].td$ is treated likewise.

Next, the variables $u^s_{l,m}$, $\mu^s_{l,m}$, $\tau_{l,m}$, and $\sigma_{l,m}$ are updated as follows:

$$u^s_{l,m} = u^e_{l,m}, \tau_{l,m} = \tau_{l,m}+1 \tag{34}$$

$$\mu^s_{l,m} = \mu^e_{l,m}, \sigma_{l,m} = \sigma_{l,m}+1 \tag{35}$$

Eqs. (18–35) are iterated until the traffic density is set for the road segment connecting l and m, and approval statuses are marked for the EVs in the prerouting and rerouting reservation queues.

3.4. AMoD Matching Service

As mentioned before, this work prohibits late-booking EVs from traversing through a saturated road segment during peak periods. Meanwhile, HDVs are disallowed to drive on expressways during peak periods to keep traffic flows of expressways under control. Accordingly, this work allows an EV owner to request a rideshare service from a designated AMoD fleet if the EV owner is pressed for time, and a CAV that matches the requirements of the EV owner will pick up the EV owner at the designated time and location.

We assume that the routes assigned for a CAV in the AMoD fleet indexed by α is expressed by a list as follows:

$$\begin{aligned}\mathscr{R}^{\alpha} = \Big\{ &\Big[\left(n^{\alpha}_{1,1}, n^{\alpha}_{1,2}\right), \left(n^{\alpha}_{1,2}, n^{\alpha}_{1,3}\right), \cdots, \left(n^{\alpha}_{1,d_1-1}, n^{\alpha}_{1,d_1}\right)\Big], \\ &\Big[\left(n^{\alpha}_{2,1}, n^{\alpha}_{2,2}\right), \left(n^{\alpha}_{2,2}, n^{\alpha}_{2,3}\right), \cdots, \left(n^{\alpha}_{2,d_2-1}, n^{\alpha}_{2,d_2}\right)\Big], \cdots, \\ &\Big[\left(n^{\alpha}_{i,1}, n^{\alpha}_{i,2}\right), \left(n^{\alpha}_{i,2}, n^{\alpha}_{i,3}\right), \cdots, \left(n^{\alpha}_{i,d_i-1}, n^{\alpha}_{i,d_i}\right)\Big], \\ &\Big[\left(n^{\alpha}_{i+1,1}, n^{\alpha}_{i+1,2}\right), \left(n^{\alpha}_{i+1,2}, n^{\alpha}_{i+1,3}\right), \cdots, \left(n^{\alpha}_{i+1,d_{i+1}-1}, n^{\alpha}_{i+1,d_{i+1}}\right)\Big], \\ &\cdots, \Big[\left(n^{\alpha}_{p,1}, n^{\alpha}_{p,2}\right), \left(n^{\alpha}_{p,2}, n^{\alpha}_{p,3}\right), \cdots, \left(n^{\alpha}_{p,d_p-1}, n^{\alpha}_{p,d_p}\right)\Big]\Big\}\end{aligned} \tag{36}$$

where the items from left to right in the list denote the following: $\mathscr{R}^{\alpha}$ indicates the sequence of the passenger pickups for a CAV indexed by α on the timeline. $n^{\alpha}_{i,j}$ denotes the jth road intersection of the ith route assigned to CAV α, and n^{α}_{i,d_i} stands for the d_ith road intersection, which is the last stop of the ith route. p is the number of the rideshare routes assigned to CAV α. Accordingly, no rideshare service is assigned to CAV α within the interval between the CAV's arrival time at n^{α}_{i,d_i} and the CAV's departure time at $n^{\alpha}_{i+1,1}$.

As shown in the top-left of Figure 2, once a rideshare request is received, this module first looks for an existing rideshare route that suits the need of the requester:

$$\begin{aligned}\underset{\alpha,i}{\text{argMin}} \Big\{ &\chi_1 \cdot \Big[\Big|(x_s, y_s) - \left(x_{n^{\alpha}_{i,j}}, y_{n^{\alpha}_{i,j}}\right)\Big| \\ &+ \Big|(x_e, y_e) - \left(x_{n^{\alpha}_{i,j+\epsilon}}, y_{n^{\alpha}_{i,j+\epsilon}}\right)\Big|\Big] + \chi_2 \cdot \left(rt_{n^{\alpha}_{i,j+\epsilon}} - rt_{n^{\alpha}_{i,j}}\right)\Big\}\end{aligned} \tag{37}$$

subject to

$$1 \le i \le rn_{\alpha}, \;\; 1 \le \epsilon \le d_i - j \tag{38}$$

$$\left|(x_s, y_s) - \left(x_{n^{\alpha}_{i,j}}, y_{n^{\alpha}_{i,j}}\right)\right| \le \Delta \tag{39}$$

$$\left|(x_e, y_e) - \left(x_{n^{\alpha}_{i,j+\epsilon}}, y_{n^{\alpha}_{i,j+\epsilon}}\right)\right| \le \Delta \tag{40}$$

$$pt_{n^{\alpha}_{i,j}} \le rt_{n^{\alpha}_{i,j}} \tag{41}$$

$$pn_{\alpha}\left(rt_{n^{\alpha}_{i,j}}\right) < pn^{max}_{\alpha} \tag{42}$$

where χ_1 and χ_2 represent the weights of the two minimization objectives set by the rideshare requester, and ϵ is a positive integer. (x_s, y_s) and (x_e, y_e) stand for the coordinates of the location of the requester's origin and the destination, respectively; whereas $\left(x_{n^{\alpha}_{i,j}}, y_{n^{\alpha}_{i,j}}\right)$, and $\left(x_{n^{\alpha}_{i,j+\epsilon}}, y_{n^{\alpha}_{i,j+\epsilon}}\right)$ denote the coordinates of the pickup point and drop-off point, respectively. Δ represents the maximal distance that is tolerable by the rideshare requester to move forward to the pickup/drop-off point. $rt_{n^{\alpha}_{i,j}}$ and $pt_{n^{\alpha}_{i,j}}$ denote the time for CAV α arriving at $n^{\alpha}_{i,j}$ and the time that the rideshare requester arrives at $n^{\alpha}_{i,j}$, respectively. rn_{α} stands for the number of the rideshare routes assigned to CAV α. $pn_{\alpha}(\cdot)$ and pn^{max}_{α} denote the number of rideshare passengers at time $rt_{n^{\alpha}_{i,j}}$ and the seating capacity of CAV α, respectively.

The first minimization objective in Eq. (37) denotes the distance that the rideshare requester moves when departing from the origin to the pickup point plus the time that the requester departs from the drop-off point to the destination. The second one represents the time required by CAV α to drive from the pickup point to the drop-off point. The weight of each optimization objective stands for the preference set by the rideshare passenger. This work first goes through the list of the rideshare routes maintained by the company operating the AMoD fleet, $\mathscr{R}^{\alpha}$, and selects the qualified candidate routes in accordance with the list of constraints given in Eqs. (38–42). Next, we derive the value inside the Min $(\cdot)$ operator in Eq. (37) for each qualified candidate route by computing the inner product of the two weights and the corresponding objectives. The candidate routes are then sorted in ascending order, based on the computation result obtained above. Accordingly, the rideshare route information for the qualified route with the smallest index in the sorted list will be delivered to the rideshare requester for reference.

If a route that fits the need of the requester is found, the information for the selected route will be sent to the rideshare requester for confirmation. In the case where no satisfactory route is available, this module assigns a CAV that is not on duty at the designated pickup time by

$$\begin{aligned}\underset{\alpha,i}{\text{argMin}} \Big\{ &\beta_1 \cdot \Big[\Big|(x_s, y_s) - \left(x_{n^{\alpha}_{i,d_i+pd_1}}, y_{n^{\alpha}_{i,d_i+pd_1}}\right)\Big| \\ &+ \Big|(x_e, y_e) - \left(x_{n^{\alpha}_{i,d_i+pd_2}}, y_{n^{\alpha}_{i,d_i+pd_2}}\right)\Big|\Big] \\ &+ \beta_2 \cdot \left(rt_{n^{\alpha}_{i,d_i+pd_2}} - pt_{n^{\alpha}_{i,d_i+pd_1}}\right)\Big\}\end{aligned} \tag{43}$$

subject to

$$rl^{\alpha} = \sum_{0 \le r < 3} \left(\sum_{pd_r \le m < pd_{r+1}} sl_{n^{\alpha}_{i,d_i+m}, n^{\alpha}_{i,d_i+m+1}} \right) \tag{44}$$

$$pd_0 = 0 \tag{45}$$

$$n^{\alpha}_{i,d_i+pd_3} = n^{\alpha}_{i+1,1} \tag{46}$$

$$rt_{n^{\alpha}_{i,d_i}} \le pt_{n^{\alpha}_{i,d_i+pd_1}} \tag{47}$$

$$rt_{n^{\alpha}_{i,d_i+pd_3}} \le rt_{n^{\alpha}_{i+1,1}} \tag{48}$$

$$\begin{aligned} & rt_{n^{\alpha}_{i,d_i+m+1}} \\ &= rt_{n^{\alpha}_{i,d_i+m}} + ID_{n^{\alpha}_{i,d_i+m},n^{\alpha}_{i,d_i+m+1}}\left(rt_{n^{\alpha}_{i,d_i+m}}\right) + \left(1-\phi_{pcs_{n^{\alpha}_{i,d_i+m}},p_j}\right) \\ &\quad \cdot \left(1-\psi_{bss_{n^{\alpha}_{i,d_i+m}},p_j}\right) \cdot SD_{n^{\alpha}_{i,d_i+m},n^{\alpha}_{i,d_i+m+1}}\left(rt_{n^{\alpha}_{i,d_i+m}}\right) + \phi_{pcs_{n^{\alpha}_{i,d_i+m}},p_j} \\ &\quad \cdot \left[ct_{pcs_{n^{\alpha}_{i,d_i+m}},p_j} + SD_{n^{\alpha}_{i,d_i+m},p_j}\left(rt_{n^{\alpha}_{i,d_i+m}}\right) + SD_{p_j,n^{\alpha}_{i,d_i+m+1}}\right. \\ &\quad \left.\left(rt_{n^{\alpha}_{i,d_i+m}} + SD_{n^{\alpha}_{i,d_i+m},p_j}\left(rt_{n^{\alpha}_{i,d_i+m}}\right)\right)\right] + \psi_{bss_{rt_{n^{\alpha}_{i,d_i+m}}},p_k} \\ &\quad \cdot \left[BSD_{bss_{n^{\alpha}_{i,d_i+m}},p_k}\left(rt_{n^{\alpha}_{i,d_i+m}}\right) + SD_{n^{\alpha}_{i,d_i+m},p_j}\left(rt_{n^{\alpha}_{i,d_i+m}}\right)\right. \\ &\quad \left. + SD_{p_k,n^{\alpha}_{i,d_i+m+1}}\left(rt_{n^{\alpha}_{i,d_i+m}} + SD_{n^{\alpha}_{i,d_i+m},p_k}\left(rt_{n^{\alpha}_{i,d_i+m}}\right)\right)\right], \\ &\quad 1 \le i \le rn_{\alpha},\ 0 \le m \le pd_3 - 1 \end{aligned} \tag{49}$$

$$\rho^{pr}_{n^{\alpha}_{i,d_i+m},n^{\alpha}_{i,d_i+m+1},np}\left(rt_{n^{\alpha}_{i,d_i+m}}\right) < \rho^{pr,max}_{n^{\alpha}_{i,d_i+m},n^{\alpha}_{i,d_i+m+1},np}\left(rt_{n^{\alpha}_{i,d_i+m}}\right),\ 1 \le np \le 3 \tag{50}$$

$$\begin{aligned} & SoC_{n^{\alpha}_{i,d_i+m+1}} \\ &= SoC_{n^{\alpha}_{i,d_i+m}} + \eta^{\alpha} \cdot \phi_{pcs_{n^{\alpha}_{i,d_i+m}},p_j} \cdot cp_{pcs_{n^{\alpha}_{i,d_i+m}},p_j} \cdot ct_{pcs_{n^{\alpha}_{i,d_i+m}},p_j} + \eta^{\alpha} \\ &\quad \cdot \theta_{wcs_{n^{\alpha}_{i,d_i+m}},n^{\alpha}_{i,d_i+m+1}} \cdot cp_{wcs_{n^{\alpha}_{i,d_i+m}},n^{\alpha}_{i,d_i+m+1}} \cdot SD_{n^{\alpha}_{i,d_i+m},n^{\alpha}_{i,d_i+m+1}}\left(rt_{c_i}\right) \\ &\quad + \psi_{bss_{n^{\alpha}_{i,d_i+m}},p_k} \cdot \left(SOC^{\alpha,max} - SoC_{n^{\alpha}_{i,d_i+m}}\right) - ap^{\alpha} \cdot sl_{n^{\alpha}_{i,d_i+m},n^{\alpha}_{i,d_i+m+1}}, \\ &\quad 1 \le i \le rn_{\alpha},\ 0 \le m \le pd_3 - 1 \end{aligned} \tag{51}$$

$$0 \le ct_{pcs_{n^{\alpha}_{i,d_i+m}},p_j} \le ct^{max}_{pcs_{n^{\alpha}_{i,d_i+m}},p_j},\ \text{if}\ \phi_{pcs_{n^{\alpha}_{i,d_i+m}},p_j} = 1 \tag{52}$$

$$SOC^{\alpha,min} \le SoC_{n^{\alpha}_{i,d_i+m}} \le SOC^{\alpha,max},\ 1 \le i \le rn_{\alpha},\ 0 \le m \le pd_3 - 1 \tag{53}$$

$$\sum_{\substack{1 \le i \le rn_{\alpha} \\ 0 \le m \le pd_3 - 1 \\ \text{if}\, SOC^{\alpha,org} - ap^{\alpha} \cdot rl^{\alpha} < SOC^{\alpha,min}}} \left(\phi_{pcs_{n^{\alpha}_{i,d_i+m}},p_j} + \theta_{wcs_{n^{\alpha}_{i,d_i+m}},n^{\alpha}_{i,d_i+m+1}} + \psi_{bss_{n^{\alpha}_{i,d_i+m}},p_k}\right) \ge 1, \tag{54}$$

$$0 \le \eta^{\alpha} \le 1 \tag{55}$$

where β_1 and β_2 represent the weights of the two minimization objectives set by the rideshare requester. $\left(x_{n^{\alpha}_{i,d_i+pd_1}}, y_{n^{\alpha}_{i,d_i+pd_1}}\right)$ and $\left(x_{n^{\alpha}_{i,d_i+pd_2}}, y_{n^{\alpha}_{i,d_i+pd_2}}\right)$ stand for the coordinates of the pickup point and drop-off point, respectively. n^{α}_{i,d_i+pd_1} and n^{α}_{i,d_i+pd_2} stand for the indices of two road intersections extending from the end of the ith route of CAV α. Notably, n^{α}_{i,d_i+pd_1} and n^{α}_{i,d_i+pd_2} correspond with the pickup and drop-off points of the rideshare requester, respectively. n^{α}_{i,d_i+pd_3} also represents the start of the $(i+1)$ th route of CAV α. Here, the route from the drop-off point of the requester to the start of $(i+1)$ th route is computed to ensure that CAV α can arrive at the start of the $(i+1)$ th route, $n^{\alpha}_{i+1,1}$, in time. $pt_{n^{\alpha}_{i,d_i+pd_1}}$ denotes the time the requester arrives at n^{α}_{i,d_i+pd_1}, and $rt_{n^{\alpha}_{i,d_i}}$ is the time that CAV α arrives at n^{α}_{i,d_i}. The definitions of the rest of the parameters are identical to those used in Eqs. (2–9).

The first minimization objective in Eq. (43) denotes the distance that the rideshare requester moves when departing from the origin to the pickup point plus the time that the requester departs from the drop-off point to the destination. The second one represents the time required by CAV α to drive from the pickup point to the drop-off point. This work first goes through $\mathscr{R}^{\alpha}$ and selects the qualified candidate routes in accordance with the list of constraints given in Eqs. (44–55). Next, we derive the value inside the Min $(\cdot)$ operator in Eq. (43) for each qualified candidate route by computing the inner product of the two weights and the corresponding objectives. The candidate routes are then sorted in ascending order, based on the computation result obtained above. Accordingly, the rideshare route information for the qualified route with the smallest index in the sorted list will be delivered to the rideshare requester for reference. In the case where no rideshare solution is available, the requester can take public transportation instead.

4. SIMULATION EXPERIMENTS

Here, we describe the experimental details and parameter settings of the proposed work. We ran a series of simulations by using the Python programing language to verify the feasibility and effectiveness of our proposed work. All experiments were performed on a personal computer built with Win10 OS, I7-10700 4.8GHz CPU and 8GB RAM.

4.1. Experimental Setup

In this section, we use the real traffic flow datasets for the experiment to evaluate the proposed work. The historical driving data were obtained from a real-time traffic information web site of the Ministry of Transportation and Communications, Taiwan [42]. The attributes of the database are the average vehicle speed and traffic density measured at the entrance of each road segment during five-minute intervals. The road segments involved in the simulations include three expressways and twelve local roads. One expressway is parallel to two other connected expressways. There is a battery-swapping station deployed at the entrance to each of the two connected expressways, and on-road wireless charging is embedded in the pavement on the paralleled expressway. Five plug-in charging stations are evenly distributed in the area that encompasses the

twelve local roads. The ratio of the number of HDVs to the number of CAVs is set as one to five, and the type of each departed EV is randomly assigned as a HDV or CAV based on this ratio. The origin and destination of each EV were generated with uniform distribution within the area encompassing the 15 road segments. The average charging time at a plug-in charging station, and the battery switching time at a battery-swapping station, are 30 minutes [43] and 3 minutes [44], respectively. The total number of records in the dataset was 12672, and the dataset was trained with SVRs. The time spent for pickup and drop-off at a road intersection was randomly set between 10 and 15 seconds. The time for an EV stopped waiting for a traffic light to turn from red to green at the entrance to each road segment was randomly set within the interval of 15 seconds. The upper limit of the traffic density permitted on each of the three expressways was set to 50 vehicles per kilometer [45].

4.2. Experimental Results and Analysis

Figure 3 illustrates the traffic volumes on the three expressways and local roads before ridesharing and traffic control strategies are applied. Expressway 3 runs parallel with the connected expressways 1 and 2. Meanwhile, only CAVs are allowed to drive on expressway 3 to ensure the speed of each CAV on expressway 3 can be dynamically adjusted by the traffic control center in this work to maintain the smooth traffic flow during rush hours. This is consistent with the presumption that a majority of EV owners tend to commute via expressway 3 owing to the permitted higher driving speed. In addition, the on-road wireless charging facility embedded in the pavement on expressway 3 also attracts the majority of EV owners because their vehicles can still drive while charging their batteries. Accordingly, this resulted in a surge of traffic volume occurring on expressway 3 during the morning and evening peak hours. In contrast, the traffic flow on local roads is relatively smoother than those of each expressway during rush hours because an EVs owner takes a route via local road(s) if the origin is nearby the destination, or if a detour is required to access an expressway.

Figure 4 shows the average travel times of EVs that correspond with the traffic volumes observed over all road segments. Notably, the travel time of an EV in the figure includes its driving time over all road segments on the route and the charging time of the EV if it needs recharging during its trip owing to a shortage of battery electricity. Recall that expressway 1 is parallel to the connected expressway 2 and expressway 3. A dramatic increase in the travel times of EVs driving on the three expressways during the typical morning and evening peak hours is evident in Figure 4, especially for expressway 3, which provides an EV with the longest high-speed travel distance on the route. Meanwhile, the length of expressway 1 is shorter than that of expressway 2, which is why the average travel time of an EV on expressway 1 is shorter than that observed on expressway 2. It can be inferred that three expressways are chosen by a large proportion of EV drivers during rush hours because this choice involves less travel time and charging time for an EV on the route to its destination. Accordingly, prolonged traffic times occur on the three expressways during the morning and evening rush hours before ridesharing and traffic control strategies are enforced. The traffic congestion on expressway 3 is more serious than it is on the other two expressways because of the favorable on-road wireless charging service embedded in the pavement on Expressway 3.

The traffic volumes that correspond with the travel times over all road segments are given in Figure 5. Compared to the original traffic volumes as given in Figure 3, the number of EVs dropped dramatically after the EV users turned to taking rideshare services offered by AMoD fleets. However, most EVs still chose the route via expressway 3, owing to it having the shortest driving time compared to other road segments, not to mention the convenience of on-road wireless charging being supported on expressway 3. Accordingly, traffic jams were still serious on expressway 3 during the morning and evening rush hours, even though the total number of EVs driving over all road segments during the two peak periods was effectively reduced.

The average travel times of EVs after utilizing the proposed AMoD rideshare service are contrasted in Figure 6. Compared with Figure 4, the traveling times of EVs on expressway 1, expressway 2, expressway 3, and local roads after utilizing AMoD rideshare service decreased 21%, 19%, 23%, and 18% on average, respectively. It can be seen that the travel times over all road segments after utilizing AMoD rideshare service improved, as expected. The reduction of the travel times of EVs traversing each expressway is more noticeable than the reduction observed on the local roads. However, traffic jams on the three expressways, especially expressway 3, are still

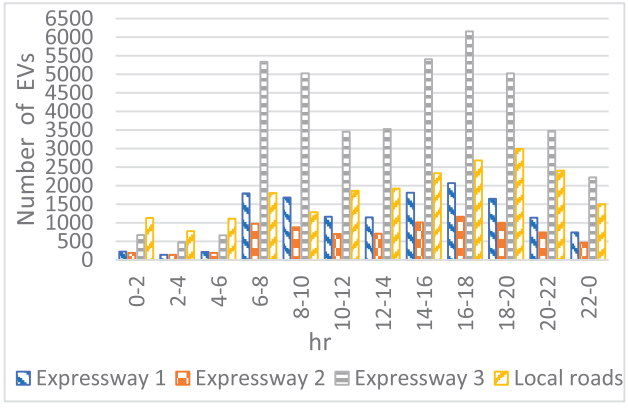

Figure 3 Original traffic volumes over the four types of road segments.

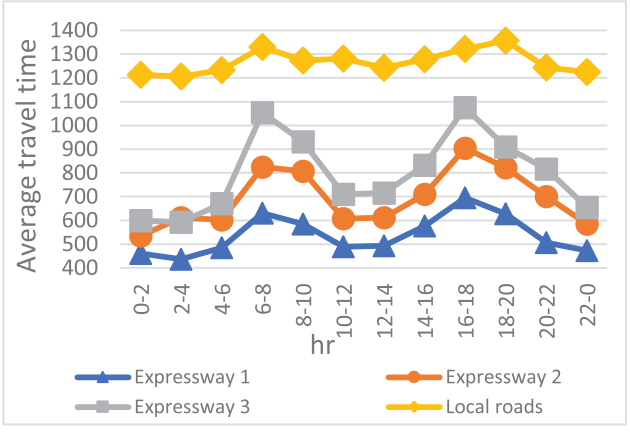

Figure 4 Original travel times of electric vehicles (EVs) over the four types of road segments.

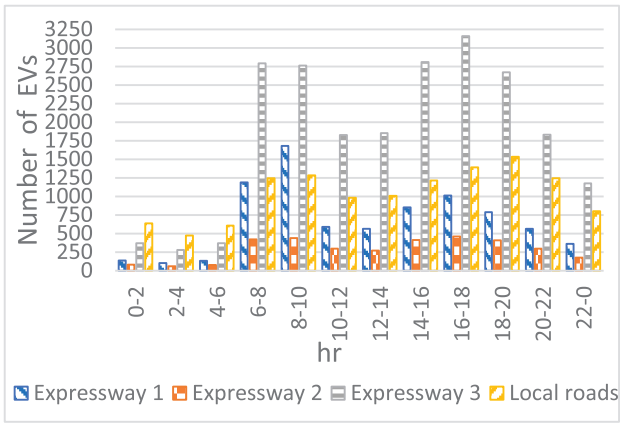

Figure 5 | Traffic volumes on the four types of road segments after invoking AMoD rideshare service.

Figure 6 | Travel times of electric vehicles (EVs) after invoking AMoD ridesharing service.

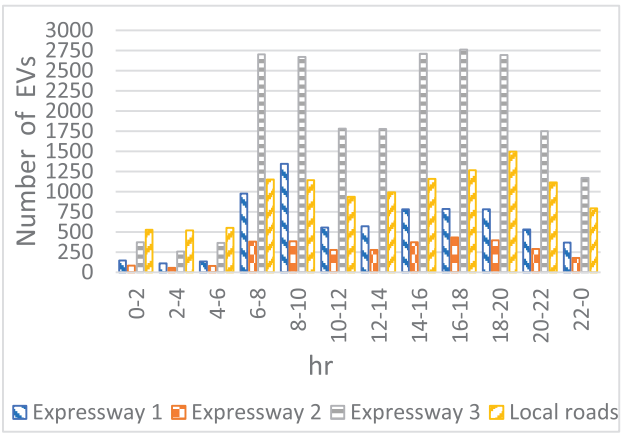

Figure 7 | Traffic volumes after implementing AMoD ridesharing plus congestion control.

Figure 8 | Travel times of electric vehicles (EVs) after implementing AMoD ridesharing plus congestion control.

apparent during rush hours because of large traffic volumes of EVs flowing onto the expressways during commute times. In contrast, the increase of the travel times of EVs on the local roads is not obvious at commute times because the traffic volumes of EVs on the local roads are not impacted to a large extent during the morning and evening peak periods.

Figure 7 gives the traffic volumes of EVs after implementing AMoD rideshare service along with appropriate traffic control strategies. The curve for the traffic volumes of EVs on expressway 3 became flat during the morning and evening rush hours. A contributing factor to this flattening is almost surely the addition of the further effect of congestion control after a sizable number of commuters opt to use AMoD rideshare services as an alternative mode of transportation for their daily commute. Although expressway 3 is still the top choice of EVs for their routes during the pre-routing and real-time rerouting processes, the late-booking EVs were allocated to alternative routes via the congestion control mechanism being enforced during the morning and evening rush hours.

Figure 8 contrasts the travel times of EVs over all road segments that correspond with the traffic volumes observed over all road segments as given in Figure 7. Compared with Figure 6, the traveling times of EVs on expressway 1, expressway 2, expressway 3, and local roads after implementing AMoD ridesharing plus congestion control decreased 9%, 7%, 12%, and 5% on average, respectively. It can be observed that the curve for the travel times of EVs on expressway 3 became much smoother during the morning and evening rush hours, owing to the congestion control being carried out on the saturated road segments during peak periods. The travel times for EVs traversing over all local roads were still much longer than those of EVs using each expressway owing to the low speed limits being enforced on local roads and traffic light delays at the local road intersections. Meanwhile, the charging time spent at the plug-in charging stations by the proportion of the EVs requiring charging prolonged the delays experienced by those EVs to some extent.

Figure 9 contrasts the average travel times of EV passengers under the three scenarios mentioned above. Compared with the original scenario, the average traveling times of EV passengers after applying the mechanisms of AMoD ridesharing and AMoD ridesharing plus congestion control decreased by 20% and 26%, respectively. To some degree, the three curves are consistent with the distribution of travel times of EVs over all types of road segments observed in the corresponding figures given above. Notably, it can be seen from this figure that the EV travel times spent on expressway 3 and on local roads dropped significantly during the morning and evening peak hours, after the proposed rideshare and traffic control strategies were put into practice. However, the disparity in the travel times between off-peak periods and peak periods cannot be overlooked

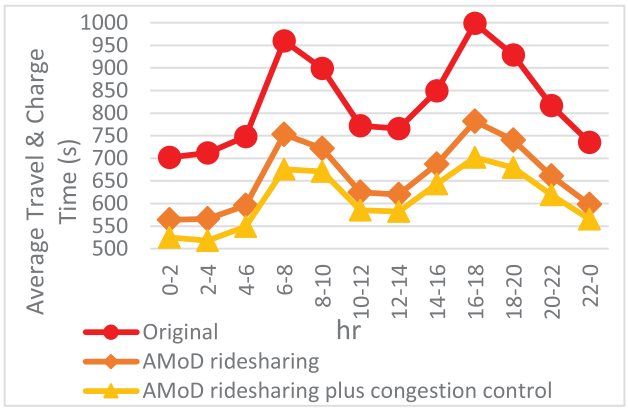

Figure 9 | Comparison of travel times of electric vehicle (EV) passengers.

because the driving speeds of CAV fleet vehicles can be automatically raised owing to the low traffic volumes of EVs over all road segments during off-peak periods.

5. CONCLUSION

To the best of our knowledge, little research work has tackled the problems of traffic congestion prevention in an urban area along with the routing and charging strategies of EVs. This work not only proposes a traffic congestion prevention mechanism for an urban area, but also accommodates the routing and charging planning for mixed traffic consisting of human-driven EVs and autonomous EVs. Each EV is required to make road segment reservations for its route before its departure time. The prerouting can be initiated via a cellphone owned by a traditional EV driver or a server installed for the management of an AMoD fleet. Then, a rerouting module will be activated at the OBU of the EV after it starts moving. The rerouting is used to respond to a situation where the EV is earlier than or delayed from the originally estimated off-peak hours to the peak hours. In the meantime, the rideshare matching service provided by an AMoD fleet is adopted to provide an alternative for an EV user who is unsatisfied with a delayed arrival time at her/his destination during the prerouting process. The simulation results indicate that this research can effectively ease the traffic congestion problem in an urban area and provide an acceptable transportation solution for EV users.

CONFLICTS OF INTEREST

The authors declare they have no conflicts of interest.

AUTHORS' CONTRIBUTIONS

Chenn-Jung Huang: conducting the research and design the algorithm. Kai-Wen Hu: Coding the algorithm. Hsing Yi Ho, Bing Zhen Xie, Chien-Chih Feng, and Hung-Wen Chuang: Reviewing and Editing.

ACKNOWLEDGMENTS

The authors would like to thank the Ministry of Science and Technology, Taiwan, for financially supporting this research under Contract Numbers MOST 108-2221-E-259-006 and MOST 109-2221-E-259-008.

REFERENCES

[1] ScienceDaily, First global study shows uneven urbanization among large cities in the last two decades, 2021. https://www.sciencedaily.com/releases/2021/01/210106095316.htm
[2] S. Çolak, A. Lima, M.C. González, Understanding congested travel in urban areas, Nat. Commun. 7 (2016), 1–8.
[3] C. Menelaou, S. Timotheou, P. Kolios, C.G. Panayiotou, M.M. Polycarpou, Minimizing traffic congestion through continuous-time route reservations with travel time predictions, IEEE Trans. Intell. Veh. 4 (2019), 141–153.
[4] A. Ahmadian, B. Mohammadi-Ivatloo, A. Elkamel, A review on plug-in electric vehicles: introduction, current status, and load modeling techniques, J. Mod. Power Syst. Clean Energy. 8 (2020), 412–425.
[5] F. Ahmad, M.S. Alam, I.S. Alsaidan, S.M. Shariff, Battery swapping station for electric vehicles: opportunities and challenges, IET Smart Grid. 3 (2020), 280–286.
[6] V. Cirimele, M. Diana, F. Bellotti, R. Berta, N. El Sayed, A. Kobeissi, *et al.*, The fabric ICT platform for managing wireless dynamic charging road lanes, IEEE Trans. Veh. Technol. 69 (2020), 2501–2512.
[7] A. Artuñedo, R.M. Del Toro, R.E. Haber, Consensus-based cooperative control based on pollution sensing and traffic information for urban traffic networks, Sensors. 17 (2017), 953.
[8] J. Godoy, J. Pérez, E. Onieva, J. Villagrá, V. Milanés, R. Haber, A driverless vehicle demonstration on motorways and in urban environments, Transport. 30 (2015), 253–263.
[9] F. Castaño, G. Beruvides, A. Villalonga, R.E. Haber, Self-tuning method for increased obstacle detection reliability based on internet of things LiDAR sensor models, Sensors. 18 (2018), 1508.
[10] T. Chu, J. Wang, L. Codecà, Z. Li, Multi-agent deep reinforcement learning for large-scale traffic signal control, IEEE Trans. Intell. Transp. Syst. 21 (2020), 1086–1095.
[11] Z. Yao, L. Shen, R. Liu, Y. Jiang, X. Yang, A dynamic predictive traffic signal control framework in a cross-sectional vehicle infrastructure integration environment, IEEE Trans. Intell. Transp. Syst. 21 (2020), 1455–1466.
[12] Z. Li, H. Yu, G. Zhang, S. Dong, C.Z. Xu, Network-wide traffic signal control optimization using a multi-agent deep reinforcement learning, Transp. Res. Part C Emerg. Technol. 125 (2021), 103059.
[13] A. Boukerche, D. Zhong, P. Sun, A novel reinforcement learning-based cooperative traffic signal system through max-pressure control, IEEE Trans. Veh. Technol. (2021).
[14] J. Mou, Intersection traffic control based on multi-objective optimization, IEEE Access. 8 (2020), 61615–61620.
[15] H. Liu, C. Claudel, R. Machemehl, K.A. Perrine, A robust traffic control model considering uncertainties in turning ratios, IEEE Trans. Intell. Transp. Syst. (2021).
[16] X. Li, P. Ye, J. Jin, F. Zhu, F.Y. Wang, Data augmented deep behavioral cloning for urban traffic control operations under a parallel learning framework, IEEE Trans. Intell. Transp. Syst. (2021).
[17] C. You, J. Lu, D. Filev, P. Tsiotras, Autonomous planning and control for intelligent vehicles in traffic, IEEE Trans. Intell. Transp. Syst. 21 (2020), 2339–2349.

[18] Y. Du, W. ShangGuan, L. Chai, A coupled vehicle-signal control method at signalized intersections in mixed traffic environment, IEEE Trans. Veh. Technol. 70 (2021), 2089–2100.
[19] S. Feng, Z. Song, Z. Li, Y. Zhang, L. Li, Robust platoon control in mixed traffic flow based on tube model predictive control, IEEE Trans. Intell. Veh. (2021).
[20] S. Bahrami, M.J. Roorda, Optimal traffic management policies for mixed human and automated traffic flows, Transp. Res. Part A Policy Pract. 135 (2020), 130–143.
[21] F. Zheng, C. Liu, X. Liu, S.E. Jabari, L. Lu, Analyzing the impact of automated vehicles on uncertainty and stability of the mixed traffic flow, Transp. Res. Part C Emerg. Technol. 112 (2020), 203–219.
[22] T. Li, F. Guo, R. Krishnan, A. Sivakumar, J. Polak, Right-of-way reallocation for mixed flow of autonomous vehicles and human driven vehicles, Transp. Res. Part C Emerg. Technol. 115 (2020), 102630.
[23] M.A.S. Kamal, T. Hayakawa, J.I. Imura, Development and evaluation of an adaptive traffic signal control scheme under a mixed-automated traffic scenario, IEEE Trans. Intell. Transp. Syst. 21 (2020), 590–602.
[24] H. Qi, R. Dai, Q. Tang, X. Hu, Coordinated intersection signal design for mixed traffic flow of human-driven and connected and autonomous vehicles, IEEE Access. 8 (2020), 26067–26084.
[25] Z. Yang, Y. Feng, H.X. Liu, A cooperative driving framework for urban arterials in mixed traffic conditions, Transp. Res. Part C Emerg. Technol. 124 (2021), 102918.
[26] A. Sharma, Z. Zheng, J. Kim, A. Bhaskar, M.M. Haque, Assessing traffic disturbance, efficiency, and safety of the mixed traffic flow of connected vehicles and traditional vehicles by considering human factors, Transp. Res. Part C Emerg. Technol. 124 (2021), 102934.
[27] L. Guo, Y. Jia, Anticipative and predictive control of automated vehicles in communication-constrained connected mixed traffic, IEEE Trans. Intell. Veh. (2021).
[28] N. Wu, D. Li, Y. Xi, Distributed integrated control of a mixed traffic network with urban and freeway networks, IEEE Trans. Control Syst. Technol. (2021).
[29] D. Ngoduy, N.H. Hoang, H.L. Vu, D. Watling, Multiclass dynamic system optimum solution for mixed traffic of human-driven and automated vehicles considering physical queues, Transp. Res. Part B Methodol. 145 (2021), 56–79.
[30] J. Wang, L. Lu, S. Peeta, Z. He, Optimal toll design problems under mixed traffic flow of human-driven vehicles and connected and autonomous vehicles, Transp. Res. Part C Emerg. Technol. 125 (2021), 102952.
[31] J. Zhang, Y. Pei, J. Shen, L. Wang, T. Ding, S. Wang, Charging strategy unifying spatial-temporal coordination of electric vehicles, IEEE Access. 8 (2020), 74853–74863.
[32] M. Ammous, S. Belakaria, S. Sorour, A. Abdel-Rahim, Joint delay and cost optimization of in-route charging for on-demand electric vehicles, IEEE Trans. Intell. Veh. 5 (2020), 149–164.
[33] A. Moradipari, M. Alizadeh, Pricing and routing mechanisms for differentiated services in an electric vehicle public charging station network, IEEE Trans. Smart Grid. 11 (2020), 1489–1499.
[34] H. Mao, J. Shi, Y. Zhou, G. Zhang, The electric vehicle routing problem with time windows and multiple recharging options, IEEE Access. 8 (2020), 114864–114875.
[35] T. Qian, C. Shao, X. Wang, M. Shahidehpour, Deep reinforcement learning for EV charging navigation by coordinating smart grid and intelligent transportation system, IEEE Trans. Smart Grid. 11 (2020), 1714–1723.
[36] R. Chen, X. Qian, L. Miao, S.V. Ukkusuri, Optimal charging facility location and capacity for electric vehicles considering route choice and charging time equilibrium, Comput. Oper. Res. 113 (2020), 104776.
[37] R. Basso, B. Kulcsár, I. Sanchez-Diaz, Electric vehicle routing problem with machine learning for energy prediction, Transp. Res. Part B Methodol. 145 (2021), 24–55.
[38] N. Chakraborty, A. Mondal, S. Mondal, Intelligent charge scheduling and eco-routing mechanism for electric vehicles: a multi-objective heuristic approach, Sustain. Cities Soc. 69 (2021), 102820.
[39] U. Bac, M. Erdem, Optimization of electric vehicle recharge schedule and routing problem with time windows and partial recharge: a comparative study for an urban logistics fleet, Sustain. Cities Soc. 70 (2021), 102883.
[40] E.Y. Kim, MRF model based real-time traffic flow prediction with support vector regression, Electron. Lett. 53 (2017), 243–245.
[41] E.Q. Martins, M.M. Pascoal, A new implementation of Yen's ranking loopless paths algorithm, Q. J. Belgian French Italian Oper. Res. Soc. 1 (2003), 121–133.
[42] Freeway Bureau, Real-time Traffic Information of Freeway Bureau, Ministry of Transportation and Communications, Taiwan. https://tisvcloud.freeway.gov.tw
[43] Pod-point, How long it takes to fully charge an electric car, 2021. https://pod-point.com/guides/driver/how-long-to-charge-an-electric-car
[44] S. Lekach, How battery swapping could reduce EV charge time to just 10 minutes, Mashable, 2021. https://mashable.com/article/ample-ev-battery-swapping-charging/
[45] G.P. Rocha Filho, R.I. Meneguette, J.R.T. Neto, A. Valejo, L. Weigang, J. Ueyama, G. Pessin, L.A. Villas, Enhancing intelligence in traffic management systems to aid in vehicle traffic congestion problems in smart cities, Ad Hoc Netw. 107 (2020), 102265.